nature communications

Article

https://doi.org/10.1038/s41467-025-59181-8

Selection of self-assembled configurational isomers from a dynamic library via a multivariant optimization process

Received: 23 September 2024

Accepted: 11 April 2025

Published online: 22 May 2025

Check for updates

Hongye Chen, Tsukasa Abe, Runyu Chai & Shuichi Hiraoka

Selection of a suitable species from a dynamic library in response to external stimuli is a key event in evolution, adaptation, and switching. The desymmetrization of building blocks enables the generation of configurational isomers for self-assembly, which is a rational approach to creating a complicated dynamic library without increasing the variety of components. However, because of their structural similarity, the selection of isomers from such a dynamic library is challenging. Here we show an artificial molecular system in which two types of self-assemblies are separately selected from a dynamic library consisting of 16 configurational isomers of hexameric cube-shaped entities assembled from C_S-symmetric gear-shaped amphiphiles upon binding two or three guest molecules. The two types of isomers were selected not only by the induced-fit selection caused by the guest molecules but also by the induction of the spatial arrangements of the guest molecules in the cluster by the assemblies. These results indicate that mutual multivariant optimization is a hidden strategy to create order from chaos in complicated systems.

A dynamic library[1–9] is reminiscent of an evolutionary process in that a certain species is selected under environmental change. Molecular self-assembly systems in which the isomers of assemblies are generated[10–15] are suitable for creating dynamic libraries. Selection in such dynamic libraries[16–19] and structural conversion[20–29] are realized by selective stabilization of one of the assemblies by an external stimulus, such as a template guest molecule and solvent, changing the relative free-energy differences among the isomers. A building block with low symmetry[30–38] enables the generation of many configurational isomers whose components are spatially arranged in different ways (Fig. 1). When a mixture of configurational isomers is generated in equilibrium, their free-energy differences are small because of their structural similarities. In such cases, an elaborate guest molecular design allows a single isomer to be differentiated from other isomers. This guest-inducing approach has been applied to the self-assembly of meal–organic cages, in which low-symmetric organic ligands are arranged in several defined ways under the requirement of complementarity between the coordination vectors of the metal ion and organic ligand[39–47]. Induced-fit selection of a single configurational isomer from a dynamic library has been achieved, but the amplification of two or more types of species separately by different guest molecules and/or conditions is challenging (Fig. 1). Such multi-adaptive behavior endows simple molecular systems with highly responsive properties for amplifying different outputs, enabling signal transduction in response to different inputs.

In a general dynamic library, a certain structure is induced by a template guest molecule. In other words, the shape of the guest molecule determines the assembled structure. When several guest molecules are accommodated in the cavity of an assembly, the spatial arrangement of the guest molecules in the cluster also contributes to the selection process. In this case, the number of guest molecules and their spatial arrangement are affected by the assembled structure (Fig. 1). Therefore, implementing such multivariant optimization in molecular systems is a significant step toward increasing complexity and would make it possible to precisely control the selection of several types of configurational isomers.

Molecular self-assembly of C_{2v}-symmetric gear-shaped amphiphile (GSA), $\mathbf{1}^{2+}$ (Fig. 2a) provides a single isomer of a cube-shaped hexameric assembly (nanocube) with an S_6 symmetry (Fig. 2b)[48,49], where the configuration of the six GSAs in each face of the cube is unambiguously determined by previous single-crystal X-ray analysis[50]

Department of Basic Science, Graduate School of Arts and Sciences, The University of Tokyo, Tokyo, Japan. e-mail: hiraoka-s@g.ecc.u-tokyo.ac.jp

https://doi.org/10.1038/s41467-025-59181-8

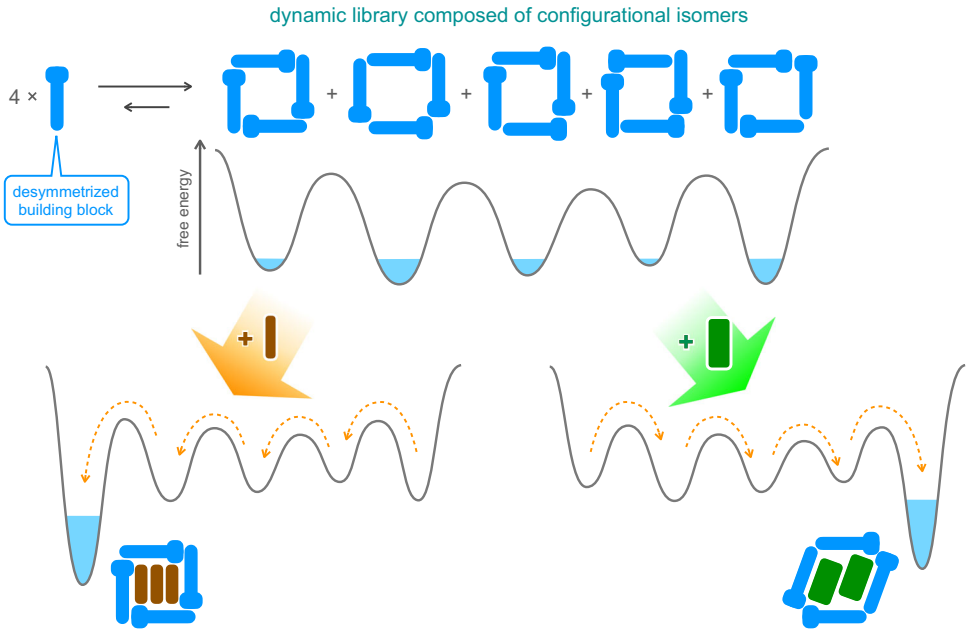

Fig. 1 | Schematic representation of multivariant optimization in a dynamic library composed of configurational isomers. The desymmetrized building blocks (blue) allow the generation of five types of configurational isomers of the assembly (square-shaped tetramers in this case). Because their free-energy differences are small, a mixture of the isomers (dynamic library) is generated. When a certain guest molecule (brown rod) two or three of which are bound in the assemblies, one type of the isomer is preferentially selected (left). In this selection process, (1) the induced configurational isomer (head-to-tail in the left), (2) the number of guest molecules (three in the left), and (3) their spatial arrangement in the cluster (stack in the left) are determined by multivariant optimization. Such an optimization process enables the selection of another configurational isomer (head-to-head) binding two slip-stacked guest molecules when a different guest molecule (green rectangle) is added (right).

(Fig. 2c). Desymmetrization of the GSA from C_{2v} into C_S symmetry ($\mathbf{1}^{2+} \rightarrow \mathbf{2}^{2+}$) generates two options for the arrangement of each GSA in the face of the cube (Fig. 2d), resulting in a dynamic library consisting of 16 configurational isomers of nanocubes (Fig. 2e and f).

Herein, we report the selection of two types of configurational isomers (*E*- and *P*-types in Fig. 2e) from a dynamic library generated via the self-assembly of C_S-symmetric GSA $\mathbf{2}^{2+}$ using different guest molecules. The two types of nanocubes differ in the size and shape of their inner cavities and were selected by different guest molecules. Because the two types of the nanocubes were induced by a cluster of guest molecules (dimer or trimer), the best isomer was found in the energy landscape by multivariant optimization of the arrangement of the GSAs in the nanocube and the arrangement of the guest molecules in the cluster. Furthermore, certain guest molecules induced both *E*- and *P*-type nanocubes, and their distributions were controlled by the concentration of the guest molecules and the temperature, leading to a different selection system in which the two types of configurational isomers were selected using one kind of guest molecules under different stimuli.

Results

Design of gear-shaped amphiphile

C_{2v}-symmetric GSA $\mathbf{1}^{2+}$ assembled into a single isomer of the nanocube, $[\mathbf{1}_6]^{12+}$, with S_6 symmetry in water (Fig. 2b and c)[49]. The driving force of this self-assembly is the hydrophobic effect, cation-π interactions between pyridinium and phenyl groups (Fig. 2g and h), and van der Waals interactions among gear-shaped hydrophobic surfaces[50–53]. In analogy to the Earth, there are the poles and the equator in the nanocube. The poles are the two vertices through which the S_6 axis penetrates, and the equator is the six sides that do not contain the pole (Fig. 2b). In order to maintain six sets of cation-π interactions (pyridinium-phenyl-pyridinium) in the nanocube (yellow and blue parts in Fig. 2g and broken lines in Fig. 2h), the arrangement of each $\mathbf{1}^{2+}$ in the face of the cube is strictly determined; Me④ in $\mathbf{1}^{2+}$ (Fig. 2a) is placed near the equator (red lines in Fig. 2c), and one of two Me④ groups is placed around the poles (Fig. 2c).

When GSA is desymmetrized into C_S by replacing one of the *p*-tolyl groups in $\mathbf{1}^{2+}$ with a methyl group to form a new GSA, $\mathbf{2}^{2+}$, there are two possibilities of the arrangement of $\mathbf{2}^{2+}$ in the face of the cube: one with Me④ near the equator (*E*-arrangement) or the other with Me④ near the pole (*P*-arrangement) (Fig. 2d). Consequently, a new GSA, $\mathbf{2}^{2+}$, generates 16 configurational isomers with *E*- or *P*-arrangement of the six GSAs in the nanocube (Fig. 2e and f). Among them, the nanocubes six GSAs of which are all *E*- or *P*-arrangement (*E*-type and *P*-type nanocubes) possess an S_6 symmetry, and all the six GSAs in them are chemically equivalent (Fig. 2e).

Synthesis of GSA and its self-assembly

GSA $\mathbf{2}\cdot Cl_2$ was synthesized according to Jux's approach[54] in 11 steps in total 3.7% yield (Supplementary Figs. 1-10). The ^{1}H NMR spectrum of $\mathbf{2}\cdot Cl_2$ in CD_3OD showed the monomer state (Fig. 3 and Supplementary Fig. 11a). When $\mathbf{2}\cdot Cl_2$ was dissolved in D_2O, a complicated, broad ^{1}H NMR spectrum was obtained (Fig. 3 and Supplementary Fig. 11b). Some of aromatic and methyl protons were upfield shifted, indicating the aggregation of the GSA by the hydrophobic effect. ^{1}H DOSY spectrum of the D_2O solution showed that all the signals have the same diffusion coefficient of 1.1×10^{-10} m^2 s^{-1} (Supplementary Fig. 12), which suggests the formation of 2-nm-sized assemblies, which is consistent of the size of the $[\mathbf{1}_6]^{12+}$ nanocube. Thus, GSA $\mathbf{2}^{2+}$ generates a dynamic library composed of the configurational isomers of the $[\mathbf{2}_6]^{12+}$ nanocube. Because of the complicated ^{1}H NMR spectrum and low sensitivity of DOSY measurements for molecules of similar sizes, the formation of oligomers other than hexamers in the library is not excluded.

Selection of two types of configurational isomers

When 1,3,5-tribromobenzene (**G1**) was added to a solution of the library, the ^{1}H NMR spectrum was dramatically changed to show a very clear ^{1}H NMR pattern (Fig. 3 and Supplementary Fig. 11c). ^{1}H DOSY spectroscopy indicated that all signals had the same diffusion coefficient of 1.2×10^{-10} m^2 s^{-1} (Supplementary Fig. 13), which corresponds to

https://doi.org/10.1038/s41467-025-59181-8

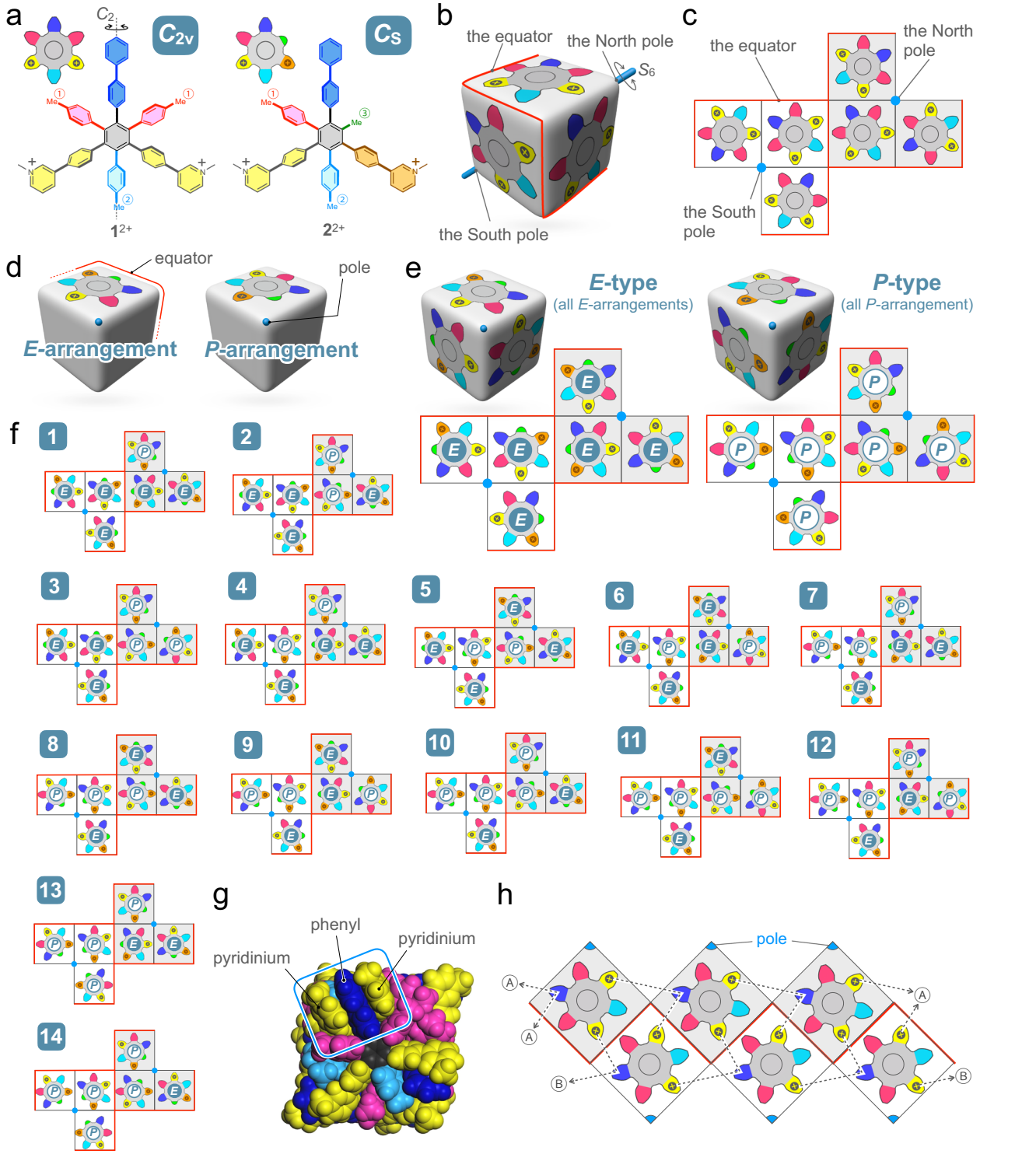

Fig. 2 | Self-assembly of cube-shaped assembly (nanocube) from gear-shaped amphiphiles (GSAs). a Chemical structures of C_{2v}- and C_S-symmetric GSAs, $\mathbf{1}^{2+}$ and $\mathbf{2}^{2+}$. **b** Schematic representation of the $[\mathbf{1}_6]^{12+}$ nanocube in analogy to the Earth. **c** The geometry net of the $[\mathbf{1}_6]^{12+}$ nanocube. **d** Two possible arrangements of a GSA in the face of the cube, *E*- and *P*-arrangements. In the *E*-arrangement, Me® (green) is located near the equator (left), whereas Me® is positioned around the pole in the *P*-arrangement (right). *E* and *P* stand for Equator and Pole, respectively **e** Two types of S_6-symmetric $[\mathbf{2}_6]^{12+}$ nanocubes, in which all six GSAs are located in *E*- or *P*-arrangement. **f** The geometry nets of possible configurational isomers except *E*- and *P*-$[\mathbf{2}_6]^{12+}$ shown in panel **e**. **g** Energy-minimized structure of $[\mathbf{1}_6]^{12+}$, in which one of six pairs of cation-π interactions working between blue and yellow aromatic rings is highlighted by a cyan rectangle. The colors of the segments of GSAs correspond to those of chemical structure of GSA $\mathbf{1}^{2+}$ shown in Fig. 2a. **h** A geometry net of the nanocube assembled from C_{2v}-symmetric $\mathbf{1}^{2+}$ to show the cation-π interactions in the triply stacked pyridinium-phenyl-pyridinium rings (broken lines).

https://doi.org/10.1038/s41467-025-59181-8

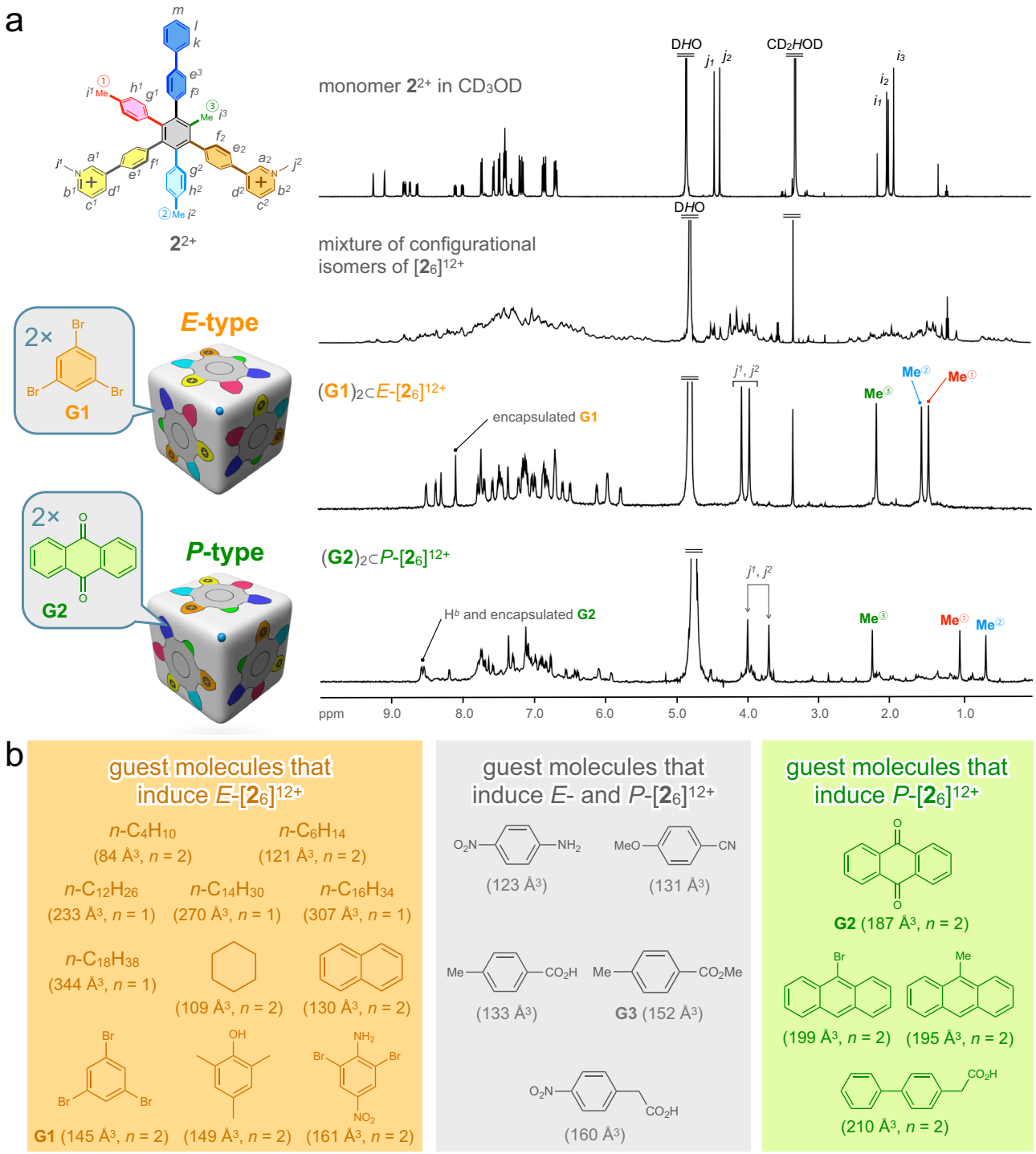

Fig. 3 | Selection of two types of configurational isomers of the nanocubes by guest molecules. a ^{1}H NMR spectra (500 MHz, 298 K) of monomer GSA (**2**$^{2+}$) in CD_3OD, a mixture of configurational isomers of the $[\mathbf{2}_6]^{12+}$ nanocubes, $(\mathbf{G1})_2\subset E$-$[\mathbf{2}_6]^{12+}$, and $(\mathbf{G2})_2\subset P$-$[\mathbf{2}_6]^{12+}$ in D_2O. The assignment of the ^{1}H NMR signals of $(\mathbf{G1})_2\subset E$-$[\mathbf{2}_6]^{12+}$, and $(\mathbf{G2})_2\subset P$-$[\mathbf{2}_6]^{12+}$ are shown in Supplementary Figs. 10c and 20, respectively. **b** List of guest molecules that induced E-$[\mathbf{2}_6]^{12+}$, P-$[\mathbf{2}_6]^{12+}$, and both types and their volumes. The volumes are indicated for a single guest molecule. The numbers of molecules encapsulated in $[\mathbf{2}_6]^{12+}$, n, are shown when determined.

an entity with 1.6 diameters. A significant feature of the ^{1}H NMR spectrum is the appearance of only one set of Me①, Me②, and Me③ signals, which indicates the selection of one type of S_6-symmetric nanocube (E- or P- type in Fig. 2f). To determine which type of nanocube was selected, ^{1}H-^{1}H NOESY spectrum was measured (Fig. 4a and Supplementary Fig. 14). The NOE between the Me③ and Me⑤ signals was observed. Because Me③ is fixed near the equator, this NOE correlation indicates that Me② is placed near the equator, which corresponds to E-type (E-$[\mathbf{2}_6]^{12+}$). The number of **G1** encapsulated in E-$[\mathbf{2}_6]^{12+}$ was determined to be two by integrating the ^{1}H signal for bound **G1**. The assignment of the ^{1}H NMR signals of $(\mathbf{G1})_2\subset E$-$[\mathbf{2}_6]^{12+}$ is shown in Supplementary Fig. 11c, which was determined by ^{1}H-^{1}H COSY and ^{1}H-^{1}H NOESY (Supplementary Figs. 14 and 15) spectroscopy. Fourier transform ion cyclotron resonance (FT-ICR) mass spectrometry (negative ion mode) of an aqueous solution of $(\mathbf{G1})_2\subset E$-$[\mathbf{2}_6]Cl_{12}$ with CH_3SO_3H as an additive detected doubly and triply charged anionic species of

https://doi.org/10.1038/s41467-025-59181-8

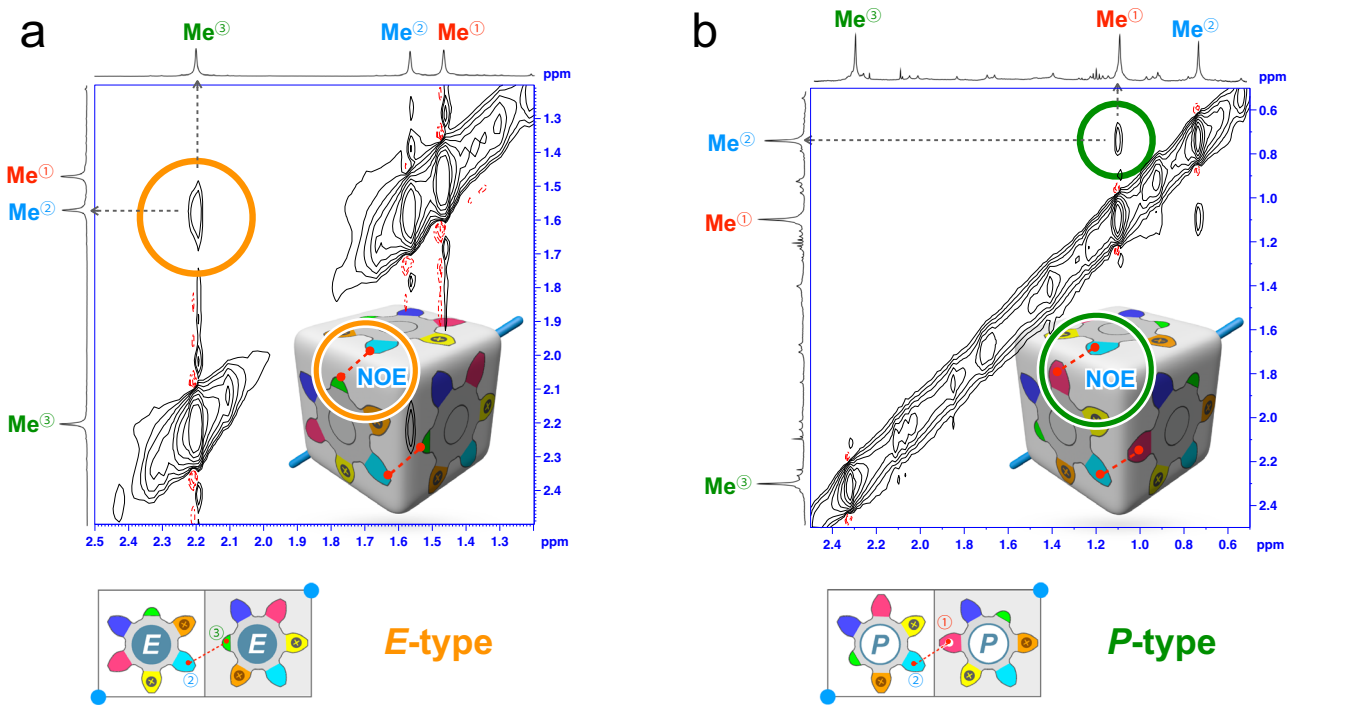

Fig. 4 | ^{1}H–^{1}H NOE spectra of *E*- and *P*-type nanocubes (500 MHz, 298 K, upfield region). a *E*-$[2_6]^{12+}$ binding two molecules of **G1**. **b** *P*-$[2_6]^{12+}$, which binds two molecules of **G2**.

$[\mathbf{2}_6(\mathrm{Cl})_x(\mathrm{CH_3SO_3})_y]^{12-x-y}$ ($x = 6$–11 and $y = 3$–9) (Supplementary Fig. 16). Unfortunately, the signals for *E*-$[\mathbf{2}_6]^{12+}$ with the bound guest molecules (**G1**) could not be detected. Other guest molecules that induced *E*-$[\mathbf{2}_6]^{12+}$ are listed in Fig. 3b and their ^{1}H NMR spectra are shown in Supplementary Figs. 17 and 18.

In the screening of guest molecules, we encountered another type of a simple ^{1}H NMR pattern when 9,10-anthraquinone (**G2**) was added to the library (Fig. 3 and Supplementary Fig. 19). ^{1}H DOSY spectroscopy indicated that all ^{1}H NMR signals showed the same diffusion coefficient of 1.1×10^{-10} m^2 s^{-1} (Supplementary Fig. 20), which corresponds to an entity with 1.7 diameters. One set of Me①, Me②, and Me③ ^{1}H NMR signals were observed, but their chemical shifts are different from those of *E*-$[\mathbf{2}_6]^{12+}$ induced by **G1**. Then, ^{1}H-^{1}H NOESY spectrum was measured to determine which type of S_6-symmentric $[\mathbf{2}_6]^{12+}$ was assembled. A D_2O solution of $\mathbf{2}^{2+}$ in the presence of **G2** showed NOE between Me① and Me② signals (Fig. 4b and Supplementary Fig. 21), indicating that Me① is placed near the equator, thus Me③ is placed near the pole, which corresponds to *P*-type (*P*-$[\mathbf{2}_6]^{12+}$). The number of **G2** encapsulated in *P*-$[\mathbf{2}_6]^{12+}$ was estimated to be two by integrating the ^{1}H NMR signal of the bound **G2** (Fig. 3a). Some of the ^{1}H NMR signals of $(\mathbf{G2})_2\subset$*P*- $[\mathbf{2}_6]^{12+}$ were assigned by ^{1}H-^{1}H COSY and ^{1}H-^{1}H NOESY spectroscopy (Supplementary Figs. 21 and 22). FT-ICR mass spectrometry of an aqueous solution of $(\mathbf{G2})_2\subset P$-$[\mathbf{2}_6]\mathrm{Cl}_{12}$ was also conducted under the same conditions as *E*-$[\mathbf{2}_6]\mathrm{Cl}_{12}$. Although the signals of the doubly and triply charged anionic species of the free nanocubes were detected, the signals of the host-guest complex could not be found (Supplementary Fig. 23). Other guest molecules that induced *P*-$[\mathbf{2}_6]^{12+}$ are listed in Fig. 3b and their ^{1}H NMR spectra are shown in Supplementary Fig. 24. Consequently, two types of configurational isomers were separately selected from an artificial dynamic library using different guest molecules.

Two types of S_6-symmetric nanocubes (*E*-$[\mathbf{2}_6]^{12+}$ and *P*-$[\mathbf{2}_6]^{12+}$) were selected by different guest molecules (**G1** and **G2**). The difference between *E*-$[\mathbf{2}_6]^{12+}$ and *P*-$[\mathbf{2}_6]^{12+}$ stems from the position of Me③ near the pole or equator (Fig. 2f), which would affect the size and shape of the nanocubes and their cavities. In the original $[\mathbf{1}_6]^{12+}$ nanocube, 12 *p*-tolyl methyl groups (six Me① and six Me②) are placed near the equator (Fig. 2c). The same is true in *P*-$[\mathbf{2}_6]^{12+}$, whereas six Me② and six Me③ are near the equator in *E*-$[\mathbf{2}_6]^{12+}$ (Fig. 2f). Thus, geometric interactions of the GSAs near the equator in *P*-$[\mathbf{2}_6]^{12+}$ would be similar to those of $[\mathbf{1}_6]^{12+}$. Attempts of single crystallization of the two types of nanocubes under various conditions failed, so the difference between *E*-$[\mathbf{2}_6]^{12+}$ and *P*-$[\mathbf{2}_6]^{12+}$ was discussed based on their optimized structures, comparing with $[\mathbf{1}_6]^{12+}$ with a spherical cavity (Fig. 5c). *E*-$[\mathbf{2}_6]^{12+}$ is a closed structure where the holes around the poles are very small (Fig. 5a), whereas *P*-$[\mathbf{2}_6]^{12+}$ has large openings around the poles (Fig. 5b).

The cavity size of *E*-$[\mathbf{2}_6]^{12+}$, 513.1 Å^3, is smaller than that of $[\mathbf{1}_6]^{12+}$, 562.0 Å^3, whereas that of *P*-$[\mathbf{2}_6]^{12+}$, 599.2 Å^3, is larger than that of $[\mathbf{1}_6]^{12+}$ (Table 1). The spatial arrangement of the six GSAs in the nanocubes can be assessed by the equator length which is defined as the sum of six sides of the hexagonal ring created by six Me② groups along the equator (Fig. 5d). The equator lengths of *E*-$[\mathbf{2}_6]^{12+}$, 60.8 Å, is much shorter than that of $[\mathbf{1}_6]^{12+}$, 64.6 Å (Table 1), which is consistent with the smaller cavity volume of *E*-$[\mathbf{2}_6]^{12+}$ than that of $[\mathbf{1}_6]^{12+}$. Although the equator length of *P*-$[\mathbf{2}_6]^{12+}$ is shorter than that of $[\mathbf{1}_6]^{12+}$, the cavity size of *P*-$[\mathbf{2}_6]^{12+}$ is larger than that of $[\mathbf{1}_6]^{12+}$, which is probably because of large openings in *P*-$[\mathbf{2}_6]^{12+}$.

Next, the distances between the two poles (d_p) in *E*-$[\mathbf{2}_6]^{12+}$ and $[\mathbf{1}_6]^{12+}$ were compared (Table 1). d_p is defined as the distance between the two carbon atoms of the Me① groups around the poles. d_p in *E*-$[\mathbf{2}_6]^{12+}$, 20.3 Å, is similar to that in $[\mathbf{1}_6]^{12+}$, 20.6 Å. Therefore, *E*-$[\mathbf{2}_6]^{12+}$ is distorted from the cube so that the equator length becomes shorter maintaining d_p (Fig. 5e), which results in an ellipsoidal cavity. The distortion of *P*-$[\mathbf{2}_6]^{12+}$ from $[\mathbf{1}_6]^{12+}$ is smaller than that of *E*-$[\mathbf{2}_6]^{12+}$ (Supplementary Figs. 25 and 26). A large distortion of *E*-$[\mathbf{2}_6]^{12+}$ from the cube is mainly due to the lack of six *p*-tolyl groups in the equator. These results indicate that the partial structure located near the equator strongly affects the nanocube structure.

It should be noted that because the GSAs in the nanocubes only mesh with each other without directional bonds, the nanocubes has high adaptability, changing the size and shape of their inner cavities in response to the guest molecules[55]. Thus, the cavity sizes of the nanocubes are variable in certain ranges. We investigated the relationship

https://doi.org/10.1038/s41467-025-59181-8

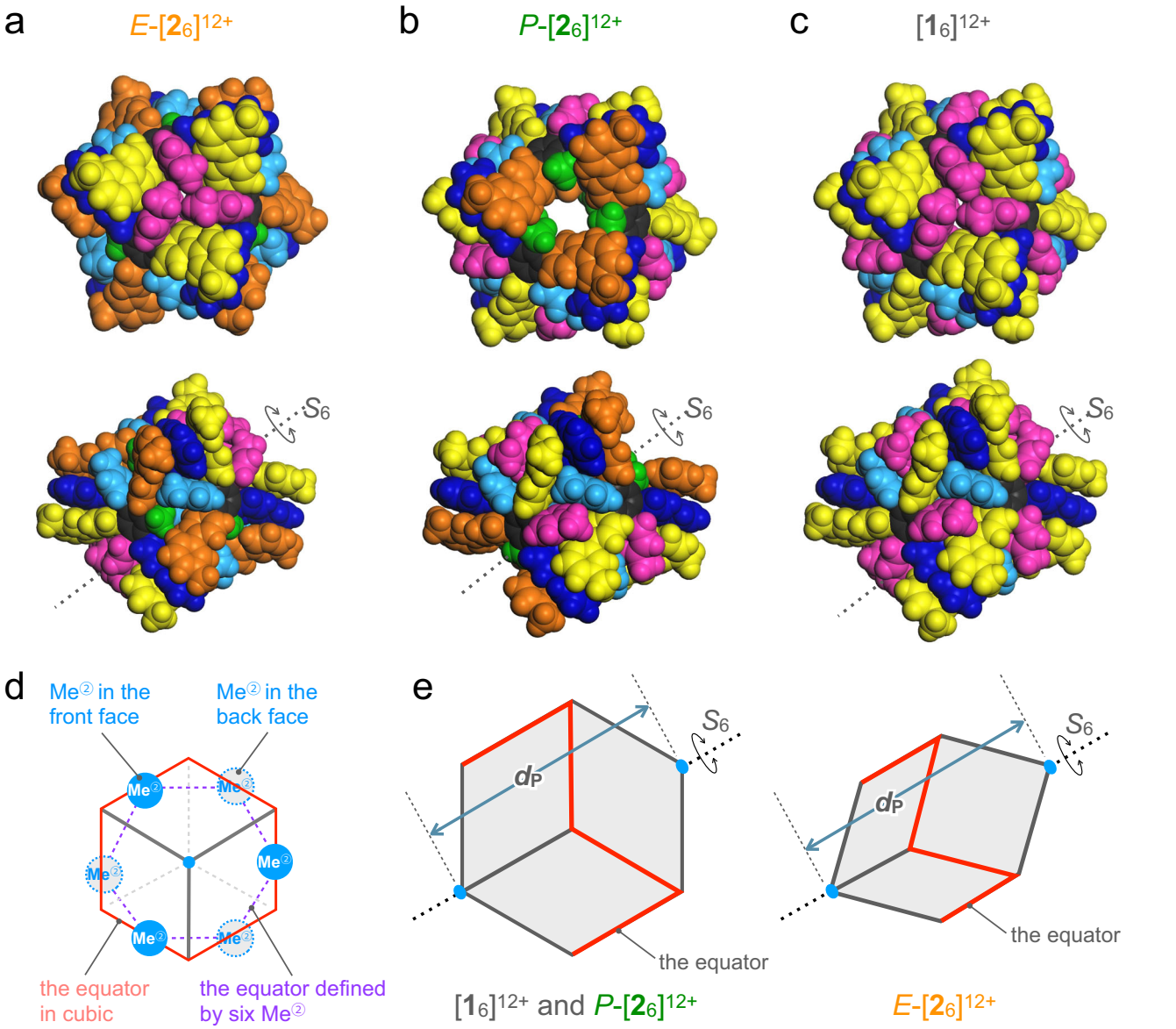

Fig. 5 | Structures of nanocubes. a–c Optimized structures of (**a**) *E*-$[\mathbf{2}_6]^{12+}$, (**b**) *P*-$[\mathbf{2}_6]^{12+}$, and (**c**) $[\mathbf{1}_6]^{12+}$. Views from the pole (above) and from the equator (below) are shown. The colors of the segments of GSAs correspond to those of chemical structure of GSA $\mathbf{2}^{2+}$ shown in Fig. 2a. **d** Definition of the equator length (purple broken line). **e** Schematic representation of cube-shaped $[\mathbf{1}_6]^{12+}$ and *P*-$[\mathbf{1}_6]^{12+}$ and a distorted cube of *E*-$[\mathbf{2}_6]^{12+}$.

between the cavity volumes and total guest volumes based on the energy-minimized structures of the *E*-and *P*-nanocubes obtained by molecular mechanics calculations (Supplementary Tables 1 and 2). The cavity volume of *E*-$[\mathbf{2}_6]^{12+}$ ranged from 471 to 536 Å^3, whereas that of *P*-$[\mathbf{2}_6]^{12+}$ ranged from 655 to 731 Å^3, exhibiting a rough linear correlation with the total guest volume (Fig. 6a). This result indicates that $[\mathbf{2}_6]^{12+}$ is highly adaptive, consistent with our previous study on $[\mathbf{1}_6]^{12+}$. The average occupancies of the guest molecules in the cavities of *E*- and *P*-$[\mathbf{2}_6]^{12+}$ are 52.9 ± 8.3% and 57.9 ± 1.8%, respectively, which are consistent with Rebek's 55% rule[56].

Table 1 | List of inner volume and equator length of nanocubes

	$[\mathbf{1}_6]^{12+}$	*E*-$[\mathbf{2}_6]^{12+}$	*P*-$[\mathbf{2}_6]^{12+}$
cavity volume[a]	562.0 Å^3	513.1 Å^3	599.2 Å^3
equator length[b]	64.6 Å	60.8 Å	63.1 Å
d_P[c]	20.6 Å	20.3 Å	n.d.[d]

[a]The cavities of the optimized structures of the nanocubes were created as inner void spaces isolated by the Connolly surface of the nanocube (Connolly radius = 1.4 Å), and their volumes were calculated.
[b]The equator length was defined in Fig. 5d.
[c]d_P is the distance between the two poles and was defined as the average distance between the two *p*-tolyl methyl carbons.
[d]not determined because the *P*-type nanocube does not have *p*-tolyl groups around the poles.

Interconversion between two types of configurational isomers

We found some of guest molecules induced both *E*-$[\mathbf{2}_6]^{12+}$ and *P*-$[\mathbf{2}_6]^{12+}$ (Figs. 3b and 7). As an example, when 4 equiv. of **G3** was added to the library, *E*-$[\mathbf{2}_6]^{12+}$ was mainly induced (Fig. 6b and Supplementary Fig. 27), whereas excess **G3** induced *P*-$[\mathbf{2}_6]^{12+}$. Considering that the cavity volume of *P*-$[\mathbf{2}_6]^{12+}$ is larger than that of *E*-$[\mathbf{2}_6]^{12+}$, the numbers of guest molecules encapsulated in *E*-$[\mathbf{2}_6]^{12+}$ and *P*-$[\mathbf{2}_6]^{12+}$ would be different. In this equilibrium (Fig. 7a and Eq. 1), high concentrations of **G3** prefer *P*-$[\mathbf{2}_6]^{12+}$.

$$(\mathbf{G3})_2 \subset E-[\mathbf{2}_6]^{12+} + \mathbf{G3} \rightleftarrows (\mathbf{G3})_3 \subset P-[\mathbf{2}_6]^{12+} \quad (1)$$

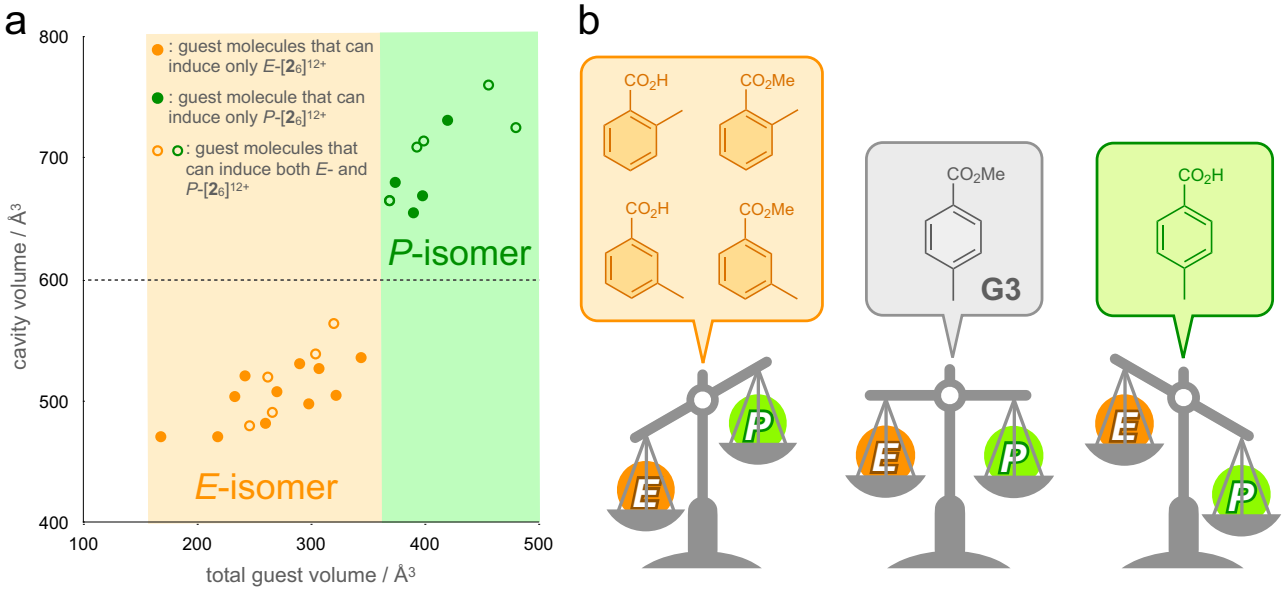

Fig. 6 | Relationship between the cavity volume and shape of the *E*- and *P*-nanocube and guest molecules. a Plot of the cavity volume of the *E*- and *P*-nanocubes versus the total guest volume of the guest molecules (Supplementary Tables 1 and 2). The cavity volumes were estimated from the energy-minimized structures of $(G)_2 \subset E\text{-}[\mathbf{2}_6]^{12+}$ and $(G)_3 \subset P\text{-}[\mathbf{2}_6]^{12+}$ using molecular mechanics calculations. There is a clear boundary between the *E*- and *P*-nanocubes in terms of the cavity volume and total guest volume. **b** The preference of the *E*- and *P*-nanocubes for disubstituted benzene derivatives. The *ortho*- and *meta*-isomers prefer the *E*-nanocube, whereas the *para*-isomer prefers the *P*-isomer. Functional groups also affect preferences. ^{1}H NMR spectra for these results are shown in Supplementary Figs. 30–35.

As the total numbers of species on the left and right sides of this equilibrium differ, temperature should affect the equilibrium. When a mixture of $E\text{-}[\mathbf{2}_6]^{12+}$ and $P\text{-}[\mathbf{2}_6]^{12+}$ in about 1:1 ratio prepared at 298 K was heated, the equilibrium shifted toward $E\text{-}[\mathbf{2}_6]^{12+}$ (Fig. 7c and Supplementary Fig. 28). The thermodynamic parameters of the equation were determined by van't Hoff analysis ($\Delta H = -36.8$ kJ mol^{-1} and $\Delta S = -81.5$ J mol^{-1} K^{-1}) (Supplementary Fig. 29), indicating that $P\text{-}[\mathbf{2}_6]^{12+}$ is entropically disfavored compared with $E\text{-}[\mathbf{2}_6]^{12+}$, which is consistent with the idea that the numbers of **G3** encapsulated in the two types of nanocubes are different.

The numbers of **G3** in the two types of $[\mathbf{2}_6]^{12+}$ could not be determined by ^{1}H NMR spectroscopy because the ^{1}H NMR signals of bound **G3** were not observed (Fig. 7b). This might be due to fast exchange of the guests between in and out of the nanocubes on the NMR time scale. Based on the volume of **G3**, 152 Å^3, two (304 Å^3) and three (456 Å^3) molecules would be encapsulated in $E\text{-}[\mathbf{2}_6]^{12+}$ and $P\text{-}[\mathbf{2}_6]^{12+}$, respectively. Other molecules that induced both *E*- and *P*-type isomers similar to **G3** are listed in Fig. 3b (Supplementary Fig. 30). Under the assumption that two and three guest molecules are encapsulated in *E*- and $P\text{-}[\mathbf{2}_6]^{12+}$, respectively, the cavity volumes of $(G)_2 \subset E\text{-}[\mathbf{2}_6]^{12+}$and $(G)_3 \subset P\text{-}[\mathbf{2}_6]^{12+}$ were calculated from the energy-minimized structures. The cavity volumes linearly correlated with the total guest volumes (Fig. 6a), and the occupancy of the cavity by the guest molecules in *E*- and $P\text{-}[\mathbf{2}_6]^{12+}$ ranged from 53.8 ± 2.6% and 58.1 ± 4.0%, respectively. These results are consistent with Rebek's 55% rule and support the assumption that two and three guest molecules are bound in *E*- and $P\text{-}[\mathbf{2}_6]^{12+}$.

Focusing on the guest molecules two or three of which are encapsulated in $E\text{-}[\mathbf{2}_6]^{12+}$ and $P\text{-}[\mathbf{2}_6]^{12+}$ (Fig. 3b), guest molecules whose volumes ranged from 84 to 161 Å^3 tend to induce $E\text{-}[\mathbf{2}_6]^{12+}$, whereas large guest molecules with volumes of 187–210 Å^3 prefer $P\text{-}[\mathbf{2}_6]^{12+}$, and guest molecules with intermediate volumes (123–160 Å^3) induced both *E*- and *P*-nanocubes. This result is consistent with the difference in cavity size between them. However, the boundary between the guest molecules that induce *E*- or *P*-nanocube and those that induce both *E*- and *P*-nanocubes is unclear. This is mainly because the shape of the guest cluster, which is induced by the nanocubes, also plays a key role in the selection of the configurational isomers.

To confirm this idea, *ortho*-, *meta*-, and *para*-isomers of disubstituted benzene derivatives were investigated for the induction of the *E*- and *P*-isomers (Fig. 6b). As mentioned above, **G3** (methyl *para*-toluate) induces both *E*- and *P*-isomers (Fig. 7). The volumes of *ortho*- and *meta*- toluates are very similar to that of *para*-toluate, but *ortho*- and *meta*- toluates induced only the *E*-nanocube (Supplementary Figs. 31–33). This result indicates that not only the total volume of the guest cluster but also its shape affects the selection process and that rod-shaped guest molecules (*para*-isomers) can induce both *E*- and *P*-nanocubes (Fig. 3b). It was found that toluic acid isomers exhibit different preferences (Fig. 6b and Supplementary Figs. 34–36). Like methyl *ortho*-toluate, *ortho*-toluic acid induced only the *E*-nanocube. *meta*-Tolic acid mainly induced the *E*-nanocube, but its induction ability was weaker than that of *ortho*-toluic acid. *para*-Toluic acid induced mainly the *P*-nanocube and did not show switching of the induction of the *E*- and *P*-nanocubes depending on the guest concentration. These results indicate that functional groups (carboxylic acid and ester) also affect the selection of the two types of nanocubes and that such a complicated multivariant optimization process realizes the selection of two types of configurational isomers.

Discussion

In conclusion, a dynamic combinatorial library of configurational isomers for molecular self-assembly was created by the rational design of a low-symmetric gear-shaped amphiphile, $\mathbf{2}^{2+}$. Without an external stimulus, a complicated mixture of 16 configurational isomers was generated. Upon adding **G1** to the library, an *E*-type nanocube ($E\text{-}[\mathbf{2}_6]^{12+}$) was selected exclusively. The cavity of $E\text{-}[\mathbf{2}_6]^{12+}$ is smaller than that of the original $[\mathbf{1}_6]^{12+}$, and its shape is ellipsoid because of the distortion of $E\text{-}[\mathbf{2}_6]^{12+}$. In contrast, **G2** selectively induced $P\text{-}[\mathbf{2}_6]^{12+}$, whose structure is similar to $[\mathbf{1}_6]^{12}$. The structural difference between $E\text{-}[\mathbf{2}_6]^{12+}$ and $P\text{-}[\mathbf{2}_6]^{12+}$ originates from the difference in meshing among the six GSAs near the equator, which resulted in differences in the size and shape of their cavities. The selection

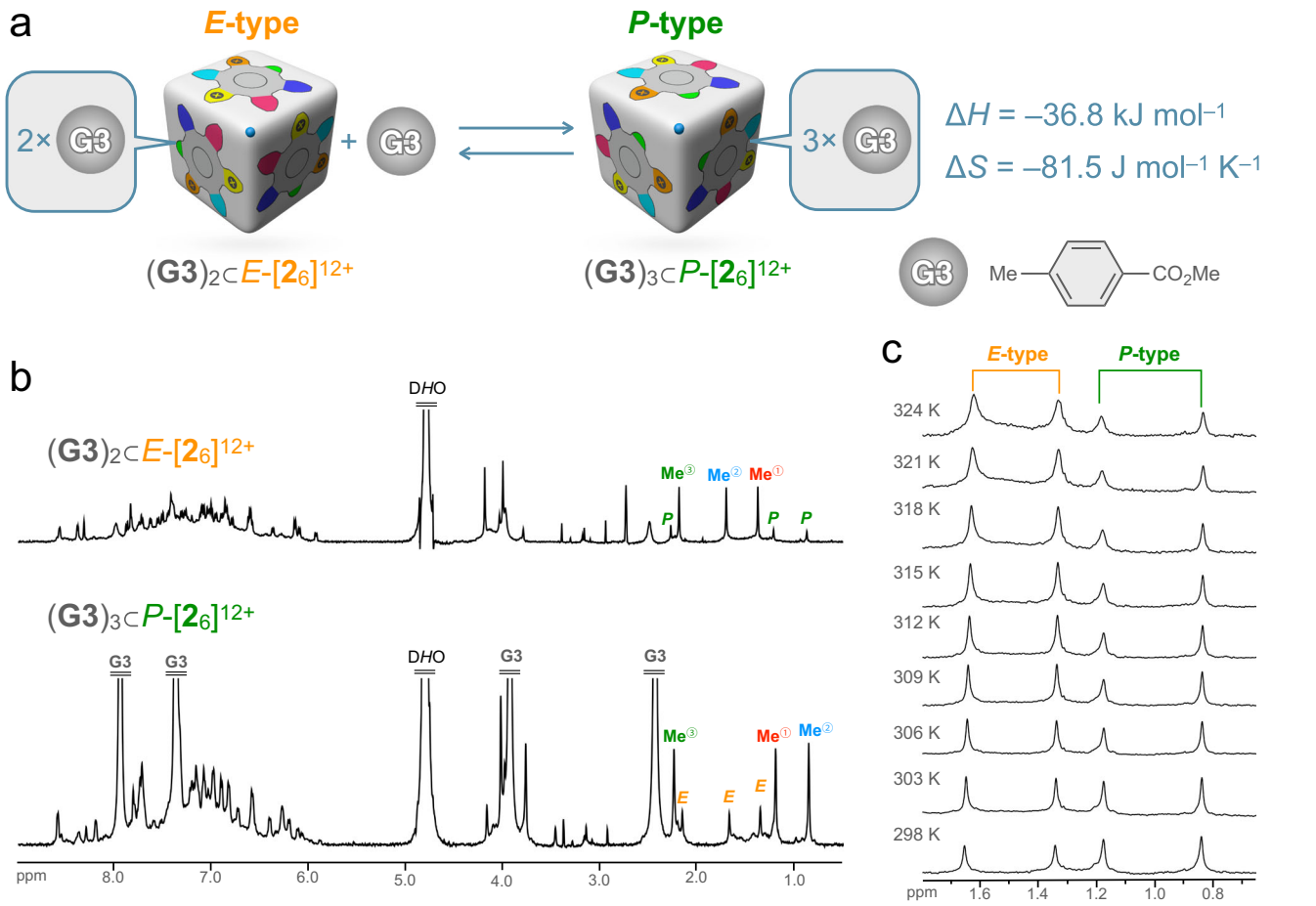

Fig. 7 | Interconversion between *E*- and *P*-types nanocubes by change in the concentration of guest molecules and the temperature. a The equilibrium between *E*- and *P*-$[\mathbf{2}_6]^{12+}$ in the presence of **G3**. **b** ^{1}H NMR spectra (500 MHz, D_2O, 298 K) of $(\mathbf{G3})_2\subset E$-$[\mathbf{2}_6]^{12+}$ and $(\mathbf{G3})_3\subset P$-$[\mathbf{2}_6]^{12+}$, which were induced by the guest concentration change of **G3**. At low concentration [**G3**]/[$\mathbf{2}_6$] = 4, *E*-type was induced, whereas excess **G3** ([**G3**]/[$\mathbf{2}_6$] = 48) induced *P*-type, because the number of **G3** encapsulated in *P*-type nanocube is more than that in *E*-type. **c** The interconversion induced by the temperature change. *E*-type nanocube was preferred at high temperatures. Thermodynamic parameters of the equation in (**a**) determined by van't Hoff analysis are shown.

process in this system is complicated because the energy minimum is determined by the mutual optimization of the spatial arrangements of both the GSAs in the nanocube and the guest molecules in the guest cluster. This differs from induced-fit selection systems where a host structure is induced by a guest molecule with a defined shape. Such multivariate optimization processes are key to creating complicated phenomena in living systems.

Methods

General information

^{1}H, ^{13}C, and 2D NMR spectra were recorded using a Bruker AV-500 (500 MHz) spectrometer. Chemical data are reported in parts per million (ppm, δ scale) downfield from tetramethylsilane (δ 0.00) and are referenced to proton resonance of a residual peak, CD_3OD (δ 3.31 ppm) and D_2O (δ 4.79 ppm). The data are presented as follows: chemical shifts, multiplicity (s = singlet, d = doublet, t = triplet, q = quartet and/or multiple resonances), coupling constants in Hertz (Hz), and integration. High-resolution mass spectra (HRMS) were obtained using a Water Xevo G2-S Tof mass spectrometer. CSI FT-ICR Mass spectra were obtained using Bruker scimaX. Column chromatography was carried out with Merck Silica gel 60 (0.063–0.200 nm) otherwise noted. Gel permeation liquid chromatography (GPC) was performed using a Japan Analytical Industry LC-9204 with JAIGEL 2HR + 2.5HR columns using chloroform as a solvent. Molecular mechanics calculations were performed using Materials Studio software (BIOVIA) with COMASS III force field.

Materials

Unless otherwise noted, all solvents and reagents were obtained from commercial suppliers (TCI Co., Ltd., WAKO Pure Chemical Industries Ltd., KANTO Chemical Co., Inc. and Sigma-Aldrich Co.) and were used as received. IRA 400 J Cl© was purchased from Organo Co. and washed with hexane, CH_2Cl_2, CH_3CN, *iso*-propanol, MeOH, water, and brine twice before use.

Synthesis of gear-shaped amphiphile 2·Cl_2

GSA **2**·Cl_2 was synthesized according to Supplementary Fig. 1.

Synthesis of compound 3. A solution of Br_2 (2.8 mL, 55 mmol) in CH_3COOH (30 mL) was added dropwise into a suspension of 2-methyl-4-nitroaniline (7.6 g, 50 mmol) in CH_3COOH (100 mL). After the reaction mixture was stirred at room temperature of 12 h, then the mixture was poured into the ice water to give a yellow precipitate. The precipitate was collected by filtration, washed with H_2O, and dried in a desiccator. Compound **3** was obtained (10.6 g, 45.9 mmol, 92%) as a yellow solid. ^{1}H NMR (500 MHz, $CDCl_3$, 298 K): δ 8.28 (d, *J* = 2.5 Hz, 1H), 7.96 (d, *J* = 2.0 Hz, 1H), 4.77 (s, 2H), 2.28 (s, 3H). The spectral data were in good agreement with the previous literature[57].

Synthesis of compound 4. A suspension of compound **3** (5.1 g, 22 mmol), 4-methylphenylboronic acid (3.3 g, 24 mmol), $Pd(PPh_3)_4$ (380 mg, 0.33 mmol), Na_2CO_3 (4.7 g, 44 mmol) in mix solvent of toluene (100 mL), ethanol (20 mL), and water (30 mL) was degassed and heated at 90 °C for 12 h. After the reaction, the mixture was cooled to room temperature and quenched with water. The mixture was extracted with chloroform three times. The organic phase was washed with brine and dried over anhydrous $MgSO_4$. After filtered off to remove $MgSO_4$ and insoluble materials, the solvent was removed in vacuo. The crude product was purified by silica gel column chromatography (hexane/EtOAc = 4:1) to give product **4** (5.2 g, 21.5 mmol, 98 %) as a yellow solid. ^{1}H NMR (500 MHz, $CDCl_3$, 298 K): δ 8.00 (*d*, *J* = 2.5 Hz, 1H), 7.94 (*d*, *J* = 2.5 Hz, 1H), 7.30 (s, 4H), 4.42 (s, 2H), 2.42 (s, 3H), 2.26 (s, 3H). ^{13}C NMR (125 MHz, $CDCl_3$, 298 K): δ 148.5, 138.7, 138.3, 134.5, 130.1, 129.0, 126.3, 125.6, 124.9, 121.4, 21.4, 17.9. HR-ESI-TOF-MS (*m*/*z*): $[M + H]^+$ calcd. for $C_{14}H_{15}N_2O_2$, 243.1129; found, 243.1144.

Synthesis of compound 5. Isoamyl nitrite (4.5 mL, 33 mmol) was added dropwise to a suspension of compound **4** (5.0 g, 20.6 mmol) and $CuBr_2$ (6 g, 27 mmol) in CH_3CN (50 mL). The reaction mixture was stirred at 70 °C for 12 h. After the mixture was cooled to room temperature, quenched with 10% ammonia solution, and extracted with EtOAc, the organic phase was washed with brine and dried over anhydrous $MgSO_4$. After filtration, the solvent was removed in vacuo to give product **5** (5.7 g 18.6 mmol 90%) as a pale yellow solid. ^{1}H NMR (500 MHz, $CDCl_3$, 298 K): δ 8.08 (*d*, *J* = 2.5 Hz, 1H), 7.99 (*d*, *J* = 2.5 Hz, 1H), 7.27 (s, 4H), 2.59 (s, 3H), 2.43 (s, 3H). ^{13}C NMR (125 MHz, $CDCl_3$, 298 K): δ 146.5, 144.9, 140.9, 138.5, 137.4, 133.1, 129.2, 129.1, 123.6, 123.2, 24.7, 21.5. HR-ESI-TOF-MS (*m*/*z*): $[M]^+$ calcd. for $C_{14}H_{12}{}^{81}BrNO_2$, 307.0031; found, 307.0008.

Synthesis of compound 6. A suspension of compound **5** (5.5 g, 18 mmol), 4-biphenylboronic acid (4.3 g, 22 mmol), $Pd(PPh_3)_4$ (312 mg, 0.27 mmol), Na_2CO_3 (4.3 g, 40 mmol) in mix solvent of toluene (100 mL), ethanol (20 mL), and water (30 mL) was degassed and heated at 90 °C for 12 h. After the mixture was cooled to room temperature and quenched with water, the reaction mixture was extracted with CH_2Cl_2. The organic phase was washed with brine and dried over anhydrous $MgSO_4$. After filtration, the solvent was removed in vacuo. The crude product was purified by silica gel column chromatography (hexane/$CHCl_3$ = 4:1) to afford product **6** (6.2 g, 16.3 mmol, 91 %) as a colorless solid. ^{1}H NMR (500 MHz, $CDCl_3$, 298 K): δ 8.13 (t, *J* = 3.3 Hz, 2H), 7.61 (d, *J* = 7.5 Hz, 2H), 7.53 (d, *J* = 8.0 Hz, 2H), 7.44 (t, *J* = 7.5 Hz, 2H), 7.35 (t, *J* = 7.5 Hz, 1H), 7.09 (d, *J* = 8.0 Hz, 2H), 6.98 (s, 4H), 2.30 (s, 3H), 2.27 (s, 3H). ^{13}C NMR (125 MHz, $CDCl_3$, 298 K): δ 147.0, 146.9, 143.2, 140.5, 140.0, 138.9, 137.7, 137.0, 130.2, 129.6, 129.0, 128.8, 127.6, 127.1, 126.8, 123.5, 122.8, 21.7, 21.2. HR-ESI-TOF-MS (*m*/*z*): $[M]^+$ calcd. for $C_{26}H_{21}NO_2$, 379.1572; found, 379. 1572.

Synthesis of compound 7. A solution of compound **6** (4.6 g 12.1 mmol) and $SnCl_2{\cdot}2H_2O$ (13.5 g 60 mmol) in EtOH (50 mL) and EtOAc (50 mL) was stirred at 80 °C for 12 h. After the mixture was cooled to room temperature and quenched with ice water. The pH was adjusted to slightly alkaline conditions by the addition of 10% NaOH aqueous solution. The layers were separated, and the aqueous phase was extracted with EtOAc. The combined organic phase was washed with brine and dried over anhydrous $MgSO_4$. After filtration, the solvent was removed in vacuo to give product **7** (4.0 g, 11.4 mmol, 94 %) as a colorless solid. ^{1}H NMR (500 MHz, $CDCl_3$, 298 K): δ 7.60 (d, *J* = 7.2 Hz, 2H), 7.44 (d, *J* = 8.2 Hz, 2H), 7.41 (t, *J* = 7.7 Hz, 2H), 7.31 (t, *J* = 7.4 Hz, 1H), 7.08 (d, *J* = 8.2 Hz, 2H), 6.97 (d, *J* = 8.1 Hz, 2H), 6.92 (d, *J* = 8.0 Hz, 2H), 6.65 (d, *J* = 2.2 Hz, 1H), 6.61 (d, *J* = 2.3 Hz, 1H), 3.69 (s, 2H), 2.24 (s, 3H), 2.14 (s, 3H). ^{13}C NMR (125 MHz, $CDCl_3$, 298 K): δ 142.8, 141.1, 139.8, 137.9, 137.2, 131.66, 131.63, 131.0, 129.7, 128.8, 128.3, 127.16, 126.99, 126.3, 115.8, 114.7, 100.30, 100.14, 21.5, 21.2. HR-ESI-TOF-MS (*m*/*z*): $[M + H]^+$ calcd. for $C_{26}H_{24}N$, 350.1904; found, 350. 1875.

Synthesis of compound 8. A solution of Br_2 (1.9 mL, 37 mmol) in $CHCl_3$ (30 mL) was added dropwise into a suspension of compound **7** (3.9 g, 11.1 mmol) in CH_3COOH (60 mL) and $CHCl_3$ (30 mL). After the reaction mixture was stirred at room temperature for 12 h, the mixture was quenched with aqueous Na_2SO_3 solution. The organic layer was separated, and the aqueous layer was extracted with $CHCl_3$. The combined organic phase was washed with brine and dried over anhydrous $MgSO_4$. After filtration, the solvent was removed in vacuo to give the product **8** (5.4 g, 10.6 mmol, 96%) as a yellow solid. ^{1}H NMR (500 MHz, $CDCl_3$, 298 K): δ 7.54 (d, *J* = 7.0 Hz, 2H), 7.37-7.41 (m 4H), 7.30 (t, *J* = 7.5 Hz, 1H), 6.95 (t, *J* = 8.0 Hz, 4H), 6.86 (d, *J* = 8.0 Hz, 2H), 4.82 (s, 2H), 2.23 (s, 3H), 2.19 (s, 3H). ^{13}C NMR (125 MHz,$CDCl_3$, 298 K): δ 141.9, 141.4, 140.8, 139.9, 138.7, 138.2, 136.4, 136.0, 133.0, 131.1, 129.8, 128.8, 128.3, 127.3, 127.0, 126.2, 111.4, 108.6, 22.6, 21.4. HR-ESI-TOF-MS (*m*/*z*): $[M + H]^+$ calcd. for $C_{26}H_{22}N^{79}Br^{81}Br$, 507.0020; found, 507.0014.

Synthesis of compound 9. A suspension of compound **8** (2.2 g, 4.33 mmol), 4-(3-pyridyl)phenylboronic acid (2 g, 10 mmol), Pd(dppf)$Cl_2{\cdot}CH_2Cl_2$ (220 mg, 0.27 mmol), and K_3PO_4 (3.6 g, 17 mmol) in toluene (40 mL) and water (4 mL) was degassed and heated at 100 °C for 12 h in a sealed tube. After the mixture was cooled to room temperature and quenched with water, the reaction mixture was extracted with CH_2Cl_2. The organic phase was washed with brine and dried over anhydrous $MgSO_4$. After filtration, the solvent was removed in vacuo. The crude product was purified by silica gel column chromatography (*n*-hexane/EtOAc = 1:1) and GPC to give product **9** (1.64 g, 2.5 mmol, 58%) as a yellow solid. ^{1}H NMR (500 MHz, $CDCl_3$, 298 K): δ 8.95 (d, *J* = 1.5 Hz, 1H), 8.80 (d, *J* = 1.5 Hz, 1H), 8.62 (d, *J* = 3.5 Hz, 1H), 8.55 (d, *J* = 3.5 Hz, 1H), 7.96 (d, *J* = 8.0 Hz, 1H), 7.83 (d, *J* = 8.0, 1H), 7.76 (d, *J* = 8.0 Hz, 2H), 7.57 (t, *J* = 7.5 Hz, 4H), 7.45 (d, *J* = 8.0 Hz, 2H), 7.38–7.41 (m, 5H), 7.33–7.28 (m, 5H), 7.12 (d, *J* = 8.0 Hz, 2H), 6.74 (d, *J* = 8.0 Hz, 2H), 6.66 (d, *J* = 8.0 Hz, 2H), 3.49 (s, 2H), 2.07 (s, 3H), 1.91 (s, 3H). ^{13}C NMR (125 MHz, $CDCl_3$, 298 K): δ 148.8, 148.49, 148.45, 148.31, 141.0, 140.6, 139.1, 138.7, 138.1, 137.4, 137.0, 136.35, 136.30, 135.8, 134.75, 134.57, 134.43, 134.2, 132.1, 131.9, 131.6, 131.16, 131.00, 128.8, 128.2, 127.6, 127.12, 127.04, 126.94, 126.5, 126.1, 124.5, 123.76, 123.62, 21.2, 19.9. HR-ESI-TOF-MS (*m*/*z*): $[M + H]^+$ calcd. for $C_{48}H_{38}N_3$, 656.3061; found, 656.3069.

Synthesis of compound 10. Isoamyl nitrite (760 µL, 5.6 mmol) was added dropwise to a suspension of compound **9** (1.42 g, 2.16 mmol) and $CuBr_2$ (1.2 g, 5.4 mmol) in CH_3CN (40 mL). The reaction mixture was stirred at 70 °C for 12 h. After the mixture was cooled to room temperature and quenched with 10% NH_3 aqueous solution, the reaction mixture was extracted with EtOAc. The organic phase was washed with brine and dried over anhydrous $MgSO_4$. After filtration, the solvent was removed in vacuo. The crude product was purified by silica gel column chromatography (*n*-hexane/EtOAc = 1:1) to give the product **10** (833 mg, 1.16 mmol, 54%) as a colorless solid. ^{1}H NMR (500 MHz, $CDCl_3$, 298 K): δ 8.97 (d, *J* = 1.9 Hz, 1H), 8.81 (d, *J* = 1.9 Hz, 1H), 8.61 (dd, *J* = 4.8, 1.5 Hz, 1H), 8.54 (dd, *J* = 4.8, 1.5 Hz, 1H), 7.99 (dt, *J* = 8.0, 1.9 Hz, 1H), 7.84 (dt, *J* = 8.0, 1.9 Hz, 1H), 7.74 (d, *J* = 8.2 Hz, 2H), 7.57-7.55 (m, 2H), 7.48 (d, *J* = 8.2 Hz, 3H), 7.44-7.38 (m, 8H), 7.32-7.30 (m, 3H), 7.22 (d, *J* = 8.3 Hz, 2H), 7.10 (d, *J* = 8.2 Hz, 2H), 6.71 (d, *J* = 8.0 Hz, 2H), 6.67 (d, *J* = 8.0 Hz, 2H), 2.06 (s, 3H), 1.95 (s, 3H). ^{13}C NMR (125 MHz, $CDCl_3$, 298 K): δ 148.7, 148.5, 148.4, 148.3, 142.5, 142.3, 141.9, 141.8, 141.4, 140.7, 139.9, 139.5, 138.8, 136.81, 136.8, 136.4, 136.3, 136.1, 135.7, 135.3, 134.5, 134.3, 131.5, 131.4, 130.8, 130.7, 130.6, 130.3, 128.9, 128.9, 127.7, 127.4, 127.4, 127.0, 126.4, 126.1, 124.9, 123.7, 123.6, 21.2, 20.9. HR-ESI-TOF-MS (*m*/*z*): $[M + H]^+$ calcd. for $C_{48}H_{36}{}^{79}BrN_2$, 719.2057; found, 719.2085.

Synthesis of compound 11. A suspension of compound **10** (1050 mg, 1.46 mmol), 4-methylphenylboronic acid (992 mg, 7.3 mmol), Pd(dppf)Cl_2·CH_2Cl_2 (120 mg, 0.15 mmol), and K_3PO_4 (1.43 g, 6.7 mmol) in toluene (20 mL) and water (2 mL) was degassed and heated at 100 °C for 12 h in a sealed tube. After the mixture was cooled to room temperature and quenched with water, the reaction mixture was extracted with CH_2Cl_2. The organic phase was washed with brine and dried over anhydrous $MgSO_4$. After filtration, the solvent was removed in vacuo. The crude product was purified by silica gel column chromatography (*n*-hexane/EtOAc = 2:1) and GPC to give product **11** (233 mg, 0.32 mmol, 22%) as a yellow solid. ^{1}H NMR (500 MHz, $CDCl_3$, 298 K): δ 8.82 (d, *J* = 2.0 Hz, 1H), 8.67 (d, *J* = 2.0 Hz, 1H), 8.54 (dd, *J* = 4.8, 1.5 Hz, 1H), 8.47 (dd, *J* = 4.8, 1.5 Hz, 1H), 7.85 (dt, *J* = 8.0, 1.9 Hz, 1H), 7.70 (dt, *J* = 8.0, 1.8 Hz, 1H), 7.58 (d, *J* = 7.2 Hz, 2H), 7.46-7.39 (m, 7H), 7.34–7.29 (m, 2H), 7.24 (d, *J* = 8.3 Hz, 3H), 7.19 (d, *J* = 8.2 Hz, 2H), 7.10 (d, *J* = 8.3 Hz, 2H), 6.92 (d, *J* = 8.3 Hz, 2H), 6.76 (d, *J* = 7.4 Hz, 4H), 6.66 (dd, *J* = 7.7, 5.0 Hz, 4H), 2.06 (s, 6H), 1.99 (s, 3H). ^{13}C NMR (125 MHz, $CDCl_3$, 298 K): δ 148.40, 148.37, 148.23, 148.10, 141.6, 141.14, 141.02, 140.92, 140.64, 140.60, 140.55, 140.40, 138.50, 138.43, 137.5, 136.4, 135.2, 134.79, 134.74, 134.18, 134.01, 133.95, 132.3, 131.27, 131.14, 130.9, 128.8, 127.61, 127.58, 127.23, 127.08, 126.97, 126.37, 126.28, 126.25, 125.2, 123.58, 123.43, 21.2, 20.1. HR-ESI-TOF-MS (*m*/*z*): $[M + H]^+$ calcd. for $C_{55}H_{43}N_2$, 731.3421, found, 731.3443.

Synthesis of compound 2·I_2. MeI (852 µL, 13.7 mmol) was added to a solution of compound **11** (100 mg 0.137 mmol) in CH_2Cl_2 (5 mL). The reaction mixture was stirred at room temperature for 12 h under dark. Then the solvent was removed in vacuo to obtain the **2**·I_2 (137 mg, 99%), which was used without further purification.

Synthesis of compound 2·Cl_2. A suspension of **2**·I_2 (137 mg, 1.35 mmol) and IRA 400 J Cl© (850 mg) in water (10 mL) were stirred at room temperature for overnight. Then the suspension was filtered, and the filtrate was concentrated in vacuo. The crude material was washed by *n*-hexane, $CHCl_3$, diethyl ether, and EtOAc twice, respectively to give the product (100 mg, 0.12 mmol, 88 % in 2 steps) as a pale yellow solid. ^{1}H NMR (500 MHz, CD_3OD, 298 K): δ 9.24 (s, 1H), 9.08 (s, 1H), 8.82 (d, *J* = 5.9 Hz, 1H), 8.78 (d, *J* = 7.8 Hz, 1H), 8.73 (d, *J* = 5.9 Hz, 1H), 8.60 (s, 1H), 8.08 (t, *J* = 7.1 Hz, 1H), 7.98 (t, *J* = 6.6 Hz, 1H), 7.72 (d, *J* = 8.2 Hz, 2H), 7.53 (s, 2H), 7.47 (s, 2H), 7.39 (t, *J* = 7.8 Hz, 6H), 7.29 (t, *J* = 7.2 Hz, 1H), 7.19 (d, *J* = 7.8 Hz, 2H), 7.14 (d, *J* = 8.3 Hz, 2H), 6.87–6.83 (m, 4H), 6.68 (t, *J* = 9.1 Hz, 4H), 4.45 (s, 3H), 4.37 (s, 3H), 2.01 (s, 3H), 2.00 (s, 3H), 1.92 (s, 3H). ^{13}C NMR (125 MHz, CD_3OD, 298 K): δ 145.3, 144.97, 144.81, 144.55, 144.50, 144.2, 143.6, 143.2, 142.6, 142.13, 141.97, 141.91, 141.51, 141.44, 141.24, 140.2, 139.3, 138.75, 138.72, 136.2, 135.0, 134.1, 133.0, 132.42, 132.30, 132.25, 131.9, 131.2, 129.8, 129.01, 128.85, 128.61, 128.56, 128.3, 127.83, 127.76, 127.2, 126.5, 21.0, 20.1. HR-ESI-TOF-MS (*m*/*z*): $[M]^{2+}$ calcd. for $C_{57}H_{48}N_2$, 380.1903; found, 380.1879.

General procedure of host-guest complexation between nanocube and guest molecules

For the encapsulation of liquid guest molecules that are insoluble in water, 1 µL of guest molecule was added to a D_2O solution of a mixture of configurational isomers of nanocube, $[\mathbf{2}_6]^{12+}$ ($[\mathbf{2}^{2+}]_0$ = 1.0 mM), in an NMR tube then sonicated for 10 min. For the encapsulation of solid guest molecules, about 1 mg of the guest molecule was added to a D_2O solution of $[\mathbf{2}_6]^{12+}$ in an NMR tube. The suspension was heated at 70 °C for 2 h. For gaseous molecules, guest molecules were added through bubbling to a D_2O solution of $[\mathbf{2}_6]^{12+}$ in an NMR tube for 1 min. The nanocubes were characterized by various ^{1}H NMR measurements and CSI-FT-ICR mass spectrometry, which are shown in the Supplementary Information.

Computational details

Molecular mechanics calculations (force field: COMPASS III) and calculations of molecular volumes of guest molecules and void spaces of the nanocubes were performed using BIOVIA Materials Studio (Dassault Systèmes). The initial structures of the nanocubes (*E*-$[\mathbf{2}_6]^{12+}$ and *P*-$[\mathbf{2}_6]^{12+}$) were created from the crystal structure of the nanocube previously reported[54] by proper change of the substituents.

Data availability

Additional data are available from the corresponding author upon request.

References

1. Dydio, P., Breuil, P. R. & Reek, J. N. H. Dynamic combinatorial chemistry in chemical catalysis. *Isr. J. Chem.* **53**, 61–74 (2013).
2. Hunt, R. A. R. & Otto, S. Dynamic combinatorial libraries: new opportunities in systems chemistry. *Chem. Commun.* **47**, 847–858 (2010).
3. Lehn, J. & Eliseev, A. V. Dynamic combinatorial chemistry. *Science* **291**, 2331–2332 (2001).
4. Kubota, Y., Sakamoto, S., Yamaguchi, K. & Fujita, M. Guest-induced organization of an optimal receptor from a dynamic receptor library: spectroscopic screening. *Proc. Natl. Acad. Sci. USA* **99**, 4854–4856 (2002).
5. Li, J., Nowak, P. & Otto, S. Dynamic combinatorial libraries: from exploring molecular recognition to systems chemistry. *J. Am. Chem. Soc.* **135**, 9222–9239 (2013).
6. Lehn, J. From supramolecular chemistry towards constitutional dynamic chemistry and adaptive chemistry. *Chem. Soc. Rev.* **36**, 151–160 (2007).
7. Corbett, P. T. et al. Dynamic combinatorial chemistry. *Chem. Rev.* **106**, 3652–3711 (2006).
8. Kriebisch, C. M. E., Bergmann, A. M. & Boekhoven, J. Fuel-driven dynamic combinatorial libraries. *J. Am. Chem. Soc.* **143**, 7719–7725 (2021).
9. Cougnon, F. B. L. & Sanders, J. K. M. Evolution of dynamic combinatorial chemistry. *Acc. Chem. Res.* **45**, 2211–2221 (2011).
10. West, K. R., Bake, K. D. & Otto, S. Dynamic combinatorial libraries of disulfide cages in water. *Org. Lett.* **7**, 2615–2618 (2005).
11. Otto, S. & Kubik, S. Dynamic combinatorial optimization of a neutral receptor that binds inorganic anions in aqueous solution. *J. Am. Chem. Soc.* **125**, 7804–7805 (2003).
12. Corbett, P. T., Sanders, J. K. M. & Otto, S. Competition between receptors in dynamic combinatorial libraries: amplification of the fittest? *J. Am. Chem. Soc.* **127**, 9390–9392 (2005).
13. Scherer, M., Caulder, D. L., Johnson, D. W. & Raymond, K. N. Triple helicate—tetrahedral cluster interconversion controlled by host–guest interactions. *Angew. Chem. Int. Ed.* **38**, 1587–1592 (1999).
14. Kieffer, M., Bilbeisi, R. A., Thoburn, J. D., Clegg, J. K. & Nitschke, J. R. Guest binding drives host redistribution in libraries of $Co^{II}_4L_4$ Cages. *Angew. Chem. Int. Ed.* **59**, 11369–11373 (2020).
15. Yamashina, M., Yuki, T., Sei, Y., Akita, M. & Yoshizawa, M. Anisotropic expansion of an M_2L_4 coordination capsule: host capability and frame rearrangement. *Chem. Eur. J.* **21**, 4200–4204 (2015).
16. Riddell, I. A. et al. Anion-induced reconstitution of a self-assembling system to express a chloride-binding $Co_{10}L_{15}$ pentagonal prism. *Nat. Chem.* **4**, 751–756 (2012).
17. Kamada, T. et al. High fidelity self-sorting assembling of meso-cinchomeronimide appended meso-meso linked Zn(II) diporphyrins. *J. Am. Chem. Soc.* **128**, 7670–7678 (2006).
18. Clegg, J. K. et al. A stimuli responsive system of self-assembled anion-binding $Fe_4L_6^{8+}$ cages. *Chem. Sci.* **4**, 68–76 (2013).
19. Hema, K. et al. Guest encapsulation alters the thermodynamic landscape of a coordination host. *J. Am. Chem. Soc.* **145**, 24755–24764 (2023).

20. Speakman, N. M. A., Heard, A. W. & Nitschke, J. R. A $Cu^{I}_{6}L_4$ cage dynamically reconfigures to form suit[4]anes and selectively bind fluorinated steroids. *J. Am. Chem. Soc.* **146**, 10234–10239 (2024).
21. Suzuki, K., Kawano, M. & Fujita, M. Solvato-controlled assembly of Pd_3L_6 and Pd_4L_8 coordination "boxes". *Angew. Chem. Int. Ed.* **46**, 2819–2822 (2007).
22. Tessarolo, J., Lee, H., Sakuda, E., Umakoshi, K. & Clever, G. H. Integrative assembly of heteroleptic tetrahedra controlled by backbone steric bulk. *J. Am. Chem. Soc.* **143**, 6339–6344 (2021).
23. Rizzuto, F. J. & Nitschke, J. R. Stereochemical plasticity modulates cooperative binding in a $Co^{II}_{12}L_6$ cuboctahedron. *Nat. Chem.* **9**, 903–908 (2017).
24. Cai, L. et al. Controlled self-assembly and multistimuli-responsive interconversions of three conjoined twin-cages. *J. Am. Chem. Soc.* **143**, 2016–2024 (2021).
25. Cheng, P. et al. Guest-reaction driven cage to conjoined twin-cage mitosis-like host transformation. *Angew. Chem. Int. Ed.* **59**, 23569–23573 (2020).
26. Xia, Z., Zhong, Y., Hu, S., Cai, L. & Sun, Q. Dynamic interconversion and induced-fit guest binding with two macrocycle-based coordination cages. *Inorg. Chem.* **62**, 8293–8299 (2023).
27. Zhang, T., Zhou, L., Guo, X., Cai, L. & Sun, Q. Adaptive self-assembly and induced-fit transformations of anion-binding metal-organic macrocycles. *Nat. Commun.* **8**, 15898 (2017).
28. Yan, D. et al. Photooxidase mimicking with adaptive coordination molecular capsules. *J. Am. Chem. Soc.* **143**, 16087–16094 (2021).
29. Walther, A., Regeni, I., Holstein, J. J. & Clever, G. H. Guest-induced reversible transformation between an azulene-based Pd_2L_4 lantern-shaped cage and a Pd_4L_8 tetrahedron. *J. Am. Chem. Soc.* **145**, 25365–25371 (2023).
30. Mishra, S. S., Kompella, S. V. K., Krishnaswamy, S., Balasubramanian, S. & Chand, D. K. Low-symmetry self-assembled coordination complexes with exclusive diastereoselectivity: experimental and computational studies. *Inorg. Chem.* **59**, 12884–12894 (2020).
31. Lewis, J. E. M. Pseudo-heterolepticity in low-symmetry metal-organic cages. *Angew. Chem. Int. Ed.* **61**, e202212392 (2022).
32. Pearcy, A. C. et al. Exploiting reduced-symmetry ligands with pyridyl and imidazole donors to construct a second-generation stimuli-responsive heterobimetallic $[PdPtL_4]^{4+}$ cage. *Chem. Sci.* **14**, 8615–8623 (2023).
33. Lewis, J. E. M. & Crowley, J. D. Metallo-supramolecular self-assembly with reduced-symmetry ligands. *ChemPlusChem* **85**, 815–827 (2020).
34. Ogata, D. & Yuasa, J. Dynamic open coordination cage from non-symmetrical imidazole–pyridine ditopic ligands for turn-on/off anion binding. *Angew. Chem. Int. Ed.* **58**, 18424–18428 (2019).
35. Lisboa, L. S., Findlay, J. A., Wright, L. J., Hartinger, C. G. & Crowley, J. D. A reduced-symmetry heterobimetallic $[PdPtL_4]^{4+}$ cage: assembly, guest binding, and stimulus-induced switching. *Angew. Chem. Int. Ed.* **59**, 11101–11107 (2020).
36. Lewis, J. E. M., Tarzia, A., White, A. J. P. & Jelfs, K. E. Conformational control of Pd_2L_4 assemblies with unsymmetrical ligands. *Chem. Sci.* **11**, 677–683 (2019).
37. Preston, D. & Evans, J. D. A lantern-shaped Pd(II) cage constructed from four different low-symmetry ligands with positional and orientational control: an ancillary pairings approach. *Angew. Chem. Int. Ed.* **62**, e202314378 (2023).
38. Mcternan, C. T., Davies, J. A. & Nitschke, J. R. Beyond Platonic: How to build metal–organic polyhedra capable of binding low-symmetry, information-rich molecular cargoes. *Chem. Rev.* **122**, 10393–10437 (2022).
39. Müller, I. M. & Möller, D. Rational design of a coordination cage with a trigonal-bipyramidal shape constructed from 33 building units. *Angew. Chem. Int. Ed.* **44**, 2969–2973 (2005).
40. Wang, X. et al. Discrete Ag_6L_6 coordination nanotubular structures based on a T-shaped pyridyl diphosphine. *Chem. Commun.* **47**, 3849–3851 (2011).
41. Birvé, A. P., Patel, H. D., Price, J. R., Bloch, W. M. & Fallon, T. Guest-dependent isomer convergence of a permanently fluxional coordination cage. *Angew. Chem. Int. Ed.* **61**, e202115468 (2022).
42. Wang, S., Sawada, T., Ohara, K., Yamaguchi, K. & Fujita, M. Capsule–capsule conversion by guest encapsulation. *Angew. Chem. Int. Ed.* **128**, 2063–2066 (2016).
43. Hiraoka, S. & Fujita, M. Guest-selected formation of Pd(II)-linked cages from a prototypical dynamic library. *J. Am. Chem. Soc.* **121**, 10239–10240 (1999).
44. Endo, K., Ube, H. & Shionoya, M. Multi-stimuli-responsive interconversion between bowl- and capsule-shaped self-assembled Zinc(II) complexes. *J. Am. Chem. Soc.* **142**, 407–416 (2019).
45. Percástegui, E. G. & Conjunto, C. Guest-induced transformations in metal-organic cages. *Eur. J. Inorg. Chem.* **43**, 4425–4438 (2021).
46. Tsutsui, T., Catti, L., Yoza, K. & Yoshizawa, M. An atropisomeric M_2L_4 cage mixture displaying guest-induced convergence and strong guest emission in water. *Chem. Sci.* **11**, 8145–8150 (2020).
47. Ronson, T. K., Carpenter, J. P. & Nitschke, J. R. Dynamic optimization of guest binding in a library of diastereomeric heteroleptic coordination cages. *Chem* **8**, 557–568 (2022).
48. Hiraoka, S., Harano, K., Shiro, M. & Shionoya, M. A self-assembled organic capsule formed from the union of six hexagram-shaped amphiphile molecules. *J. Am. Chem. Soc.* **130**, 14368–14369 (2008).
49. Zhan, Y. et al. Hyperthermostable cube-shaped assembly in water. *Commun. Chem.* **1**, 14 (2018).
50. Hiraoka, S., Nakamura, T., Shiro, M. & Shionoya, M. In-water truly monodisperse aggregation of gear-shaped amphiphiles based on hydrophobic surface engineering. *J. Am. Chem. Soc.* **132**, 13223–13225 (2010).
51. Zhan, Y. et al. Importance of molecular meshing for the stabilization of solvophobic assemblies. *J. Org. Chem.* **83**, 5132–5137 (2018).
52. Zhan, Y. et al. Polarizability and isotope effects on dispersion interactions in water. *Commun. Chem.* **2**, 141 (2019).
53. Zhan, Y., Kojima, T., Koide, T., Tachikawa, M. & Hiraoka, S. A balance between van der Waals and cation–π interactions stabilizes hydrophobic assemblies. *Chem. Eur. J.* **24**, 9130–9135 (2018).
54. Lungerich, D. et al. A strategy towards the multigram synthesis of uncommon hexaarylbenzenes. *Angew. Chem. Int. Ed.* **55**, 5602–5605 (2016).
55. Zhan, Y. et al. Induced-fit expansion and contraction of a self-assembled nanocube finely responding to neutral and anionic guests. *Nat. Commun.* **9**, 4530 (2018).
56. Mecozzi, S. & Rebek, J. Jr The 55% solution: a formula for molecular recognition in the liquid state. *Chem. Eur. J.* **4**, 1016–1022 (1998).
57. Hao, C. et al. Development of 2,4-diaminoquinazoline derivatives as potent PAK4 inhibitors by the core refinement strategy. *Eur. J. Med. Chem.* **131**, 1 (2017).

Acknowledgements

This work was supported by JSPS KAKENHI grant numbers 21K18974 and 23H01970 and the Asahi Glass Foundation. The authors thank Dr. Akio Miyazato (JAIST) for the CSI FT-ICR MS measurements.

Author contributions

S.H. conceived the project. H.C., T.A., and R.C. performed experiments. S.H., H.C., T.A., and R.C. analyzed the results and prepared the manuscript and the supplementary information. All authors discussed the results and commented on the manuscript.

Competing interests

The authors declare no competing interests.

Additional information

Supplementary information The online version contains supplementary material available at https://doi.org/10.1038/s41467-025-59181-8.

Correspondence and requests for materials should be addressed to Shuichi Hiraoka.

Peer review information *Nature Communications* thanks Qing-Fu Sun and the other anonymous reviewer(s) for their contribution to the peer review of this work. A peer review file is available."